ACS NANO

www.acsnano.org

ARTICLE

Gating of Hydrophobic Nanopores with Large Anions

Jake W. Polster, Elif Turker Acar, Fikret Aydin, Cheng Zhan, Tuan Anh Pham,* and Zuzanna S. Siwy*

Cite This: *ACS Nano* 2020, 14, 4306–4315

Read Online

ACCESS | Metrics & More | Article Recommendations | Supporting Information

ABSTRACT: **Understanding ion transport in nanoporous materials is critical to a wide variety of energy and environmental technologies, ranging from ion-selective membranes, drug delivery, and biosensing, to ion batteries and supercapacitors. While nanoscale transport is often described by continuum models that rely on a point charge description for ions and a homogeneous dielectric medium for the solvent, here, we show that transport of aqueous solutions at a hydrophobic interface can be highly dependent on the size and hydration strength of the solvated ions. Specifically, measurements of ion current through single silicon nitride nanopores that contain a hydrophobic−hydrophilic junction show that transport properties are dependent not only on applied voltage but also on the type of anion. We find that in Cl^--containing solutions the nanopores only conducted ionic current above a negative voltage threshold. On the other hand, introduction of large polarizable anions, such as Br^- and I^-, facilitated the pore wetting, making the pore conductive at all examined voltages. Molecular dynamics simulations revealed that the large anions, Br^- and I^-, have a weaker solvation shell compared to that of Cl^- and consequently were prone to migrate from the aqueous solution to the hydrophobic surface, leading to the anion accumulation responsible for pore wetting. The results are essential for designing nanoporous systems that are selective to ions of the same charge, for realization of ion-induced wetting in hydrophobic pores, as well as for a fundamental understanding on the role of ion hydration shell on the properties of solid/liquid interfaces.**

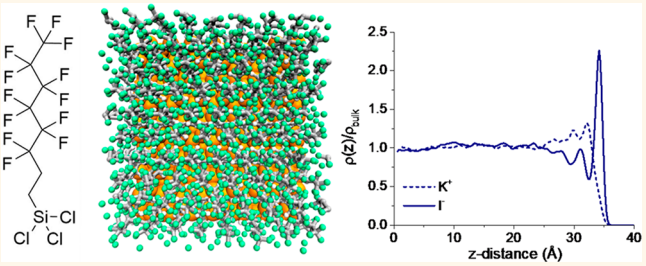

KEYWORDS: *hydrophobic interface, ion current gating, wettability, molecular dynamics simulations, first-principles calculations*

Hydrophobic interactions play an important role in many biological processes, such as protein folding and regulating transport in biological cells.[1−6] Interfaces between a hydrophobic surface and an aqueous solution were often found to exhibit many similar properties to those of the water/vapor interface,[7−12] which is amenable to a variety of spectroscopic approaches that have been employed to determine the distribution of water and ions at the interfaces.[13−15] For instance, several existing experiments and modeling[12,16−18] revealed that water density at hydrophobic surfaces was lower compared to the bulk value and that the interfacial region is dominated by large polarizable ions including iodide and bromide. On the other hand, small ions with large hydration energies, such as multivalent ions, tended to remain in the bulk solutions or exhibit weak accumulation at the interface, as observed for chloride.[16,19−22]

The remaining unresolved question considers possible consequences of the enhanced concentration of polarizable ions on transport behavior of nanoscale systems such as hydrophobic nanopores and nanochannels. Hydrophobic nanopores have attracted a great deal of research interest due to their applications in designing valves for on-demand delivery of ions and molecules, separation processes, and model systems to understand wetting/dewetting transitions at the nanoscale.[23−27] If one could gate hydrophobic nanopores with different ions, such channels would provide the basis for ion-specific responsive systems with applications in ionic circuitry and sensing.

Previous results suggested that achieving ionic gating in hydrophobic nanopores should be possible. Specifically, continuum modeling that took into account solvation energies of ions predicted that iodide ions would adsorb to a hydrophobic surface and render it negatively charged.[28] Yet, so far ionic transport through hydrophobic nanopores has been mostly studied in physiological salts, such as aqueous solutions of KCl and NaCl. In these salts, hydrophobic nanopores act like valves because they are filled with water vapor, which, in

Received: December 12, 2019
Accepted: March 17, 2020
Published: March 17, 2020

https://dx.doi.org/10.1021/acsnano.9b09777
ACS Nano 2020, 14, 4306–4315

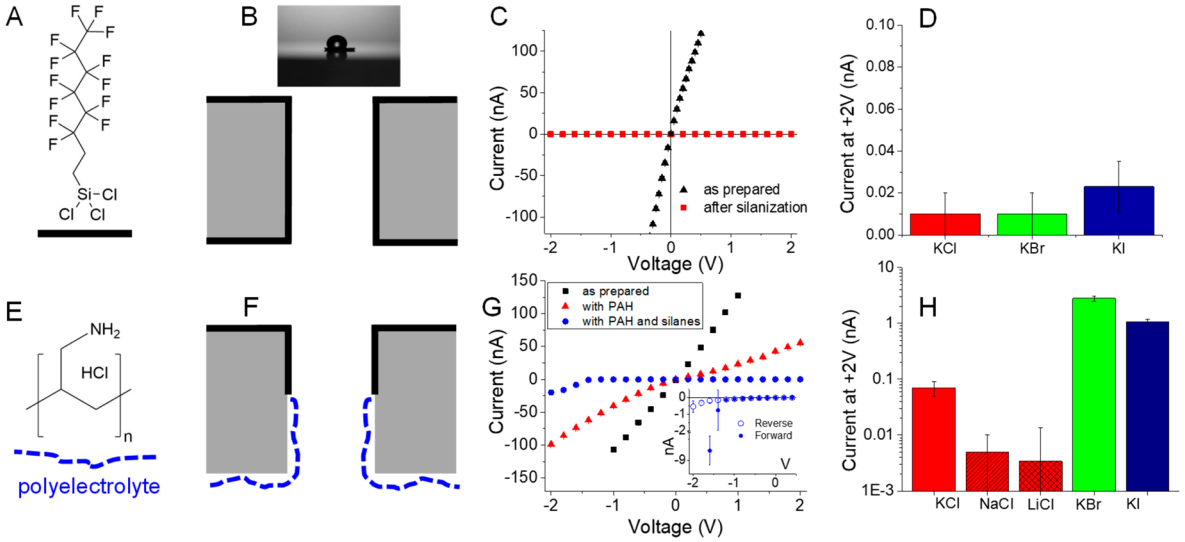

Figure 1. Preparation of hydrophobic nanopores. (A) Chemical structure of silanes used to render the silicon nitride surface hydrophobic. (B) Scheme of a nanopore subjected to symmetric silanization together with a contact angle measurement performed on a flat, silane-modified silicon nitride surface. (C) Current−voltage curves of a 50 nm diameter nanopore before and after silanization, recorded in 1 M KCl. (D) Current magnitude at +2 V recorded in 1 M KCl, KBr, and KI for the same nanopore as shown in (C). (E) Polyelectrolyte poly(allylamine hydrochloride) (PAH) used to render one pore entrance positively charged. (F) Scheme of a nanopore subjected to PAH and silanization modifications. (G) Current−voltage curves for a 25 nm diameter nanopore before and after chemical modifications. Forward scans are shown in the main panel; the inset contains a reverse scan (open symbols) and zoomed-in part of the forward scan (filled symbols) in 1 M KCl. Note that in the inset, for clarity, the voltage range only from −2 V to +0.4 V is shown, and the *y*-axis scale contains a break. (H) Summary of ion current at +2 V for the same nanopore in different salts; recordings after the PAH and silane modifications are shown. Error bars shown in panels (C), (D), (G), and (H) are standard deviations found based on ion current signals recorded at each voltage for 100 s (see Materials and Methods section). The exception is one recording in (G) shown as red triangles that was performed without time resolution using a picoammeter; average value and standard deviation at each voltage were found based on three consecutive current−voltage curves. In (C) and some recordings in (G) (shown as black and red data points) the error bars are smaller than data points.

the absence of external stimulus, prevents them from transporting ions or molecules.[3,24,25,29] Transport of water and all dissolved species in it can be, however, induced by applying a pressure difference[25,30−32] or transmembrane potential.[25,29,33−35] Ion current passing through a nanopore is the main observable informing on the nanopore wetting status: when the pore is filled with water vapor, the current is nearly zero, while wetting of the pore is observed as finite current. Using an electric field is advantageous because, in contrast to a system gated by pressure difference, applying voltage does not require mechanical strengthening of the membrane, and thus many experiments can be performed with one nanopore without its breaking. Wetting hydrophobic nanopores with an electric field has recently been explained *via* voltage-induced alignment of water dipoles, which in turn allows ions to pass through the pore and produce finite ion current.[36]

In this article we show that ionic transport through hydrophobic nanopores can be gated by a combination of electric field and large polarizable anions. To this end, we designed nanopores containing a hydrophobic entrance on one side and a hydrophilic, highly charged entrance on the other side. Such an asymmetric hydrophobic/hydrophilic junction has been shown to lower hydrophobic interactions,[37−39] allowing us to induce the wetting of nanopores for voltages below 2 V, while probing pore gating with different ion types. Our ion current measurements suggested that large polarizable anions, such as bromide and iodide, favorably adsorb to the hydrophobic interfaces and, in turn, promote the voltage-induced wetting process. We show that the wetting process enhances nanopore conductance by at least an order of magnitude in KI and KBr solutions as compared to KCl at the same concentration. On the other hand, we find that effects of selected cations on the voltage-induced wetting process were much weaker than the influence of anions. Our experimental findings were supported by first-principles calculations and molecular dynamics simulations;[40] specifically, the simulations revealed that larger anions yield weaker and less defined hydration shells and are more prone to accumulate at a hydrophobic surface where water concentration is diminished.

RESULTS AND DISCUSSION

All nanopores were prepared in 30 nm thick silicon nitride films by the dielectric breakdown process.[41,42] Pore diameter was tuned *via* controlling the magnitude of the breakthrough current measured when the dielectric breakdown process was stopped. Nanopores prepared by this technique are known to exhibit various characteristics of current−voltage curves, suggesting that their shape might not be cylindrical.[43] In order to estimate the effective pore opening diameter and to allow comparison between independently prepared nanopores, the nanopores were sized based on their conductance measured in 1 M KCl and using a cylindrical pore model with access resistance. Results presented in this article were obtained from nanopores with effective opening diameters between 10 and 140 nm.

The membranes were rendered hydrophobic by silanization reaction with 1*H*,1*H*,2*H*,2*H*-perfluorooctyltrichlorosilane.[44] Silicon nitride surfaces subjected to the modification exhibited a contact angle in water of ∼120° (Figure 1A,B); a silicon nitride surface before functionalization had a contact angle of 60° (Table S1). Two nanopores (25 and 50 nm diameter)

https://dx.doi.org/10.1021/acsnano.9b09777
ACS Nano 2020, 14, 4306−4315

were silanized symmetrically from both sides, resulting in the silanes' attachment to the entire pore wall and membrane surface. Figure 1C and Figure S1 show recordings for the 50 nm diameter nanopore before and after the silanization reaction. The pore exhibited nearly no ion current in KCl, KBr, and KI, which is consistent with the strong hydrophobic character of the pore walls (Figure 1D); the increase of the current in KI is not significant and remains within the signal noise. Recordings for the 25 nm nanopore are shown in Figure S2, which was additionally probed in NaCl and LiCl (not shown). The 25 nm pore conducted finite current only in KBr, indicating that these silanized nanopores were too resistive to achieve voltage- or ion-induced hydrophobic gating (Figure 1D, Figure S2). This conclusion was supported by experiments in KCl with 5 additional silanized nanopores, which conducted just a few tens of pA at 2 V for both voltage polarities.

In the design of hydrophobic nanopores, which would be closed for ionic transport at low voltages but would conduct ions at higher voltages, we were inspired by earlier simulations and experiments that indicated charge placement near hydrophobic groups could lower hydrophobic interactions.[37,38] The nanopores were therefore equipped with a junction between a hydrophobic pore entrance and a hydrophilic, highly charged entrance. To this end, a single-nanopore chip was first exposed from one side to a solution of positively charged polyelectrolyte, poly(allylamine hydrochloride) (PAH) (Figure 1E).[45] Due to the negative surface charges of silicon nitride, PAH was expected to electrostatically attach to the membrane surface and part of the pore walls, creating a junction between positively charged PAH and negatively charged unmodified silicon nitride. As shown before, such junctions induce ion current rectification;[46−50] thus recording asymmetric current−voltage curves indicated successful modification with PAH (Figure 1G). In the next step, the unmodified side of the membrane was subjected to silanization modification and was rendered hydrophobic, completing the proposed hydrophobic/hydrophilic junction (Figure 1F). Ionic transport properties of a nanopore containing such hydrophobic/hydrophilic junction in 1 M KCl are shown in Figure 1G. The nanopore showed nearly no conductance at all positive voltages but opened for ionic transport at negative voltages where hysteresis was observed. During the first forward scan, when voltage was changed from −2 V to +2 V with 200 mV steps, the pore started in the open−conductive state at high negative voltages and closed for ionic transport at −1.2 V, when the measured current decreased to a few tens of pA. The pore remained closed for the rest of the scan. The transition from a conductive state to a nonconductive state corresponds to a dewetting process, *i.e.*, formation of a vapor region within the pore. For the reverse scan, when the voltage was changed from +2 V to −2 V, the pore opened for ionic transport only at −1.6 V (see the inset in Figure 1G); this transition corresponds to filling the pore with condensed water. The existence of the hysteresis such that voltage needed to open the pore for ionic transport (−1.6 V) was higher than the voltage magnitude (−1.2 V) at which the pore underwent dewetting (nearly zero conductance) is consistent with earlier observations with hydrophobic nanopores.[51] Note that the pore opened for ionic transport in KCl only for negative voltages, thus when anions were sourced from the side with positively charged PAH and moved toward the silanized side of the membrane.

The same nanopore was also examined in 1 M NaCl and LiCl, as well as KBr and KI, to probe the influence of cations and anions on the voltage dependence of ion current and nanopore wetting. Figure 1H summarizes the results and shows ion currents at +2 V, the condition most sensitive to the wetting transition. In our electrode configuration, hydrophobic nanopores exhibit negligible conductance in KCl at positive voltages. Thus, finite values of positive currents could indicate diminished hydrophobic interactions and pore wetting. The recordings in Figure 1H clearly display a large current increase in bromide and iodide solutions, while no significant increase for currents in sodium and lithium solutions was observed. The series of experiments suggested that the presence of large polarizable ions in the solution indeed influenced the solid/liquid interface and promoted the process of nanopore wetting. Figure S4 shows ion currents for all salts at −2 V; due to finite conductance of this nanopore in KCl, the wetting effect of Br^- and I^- was less visible compared to the recordings at +2 V. Similar to ion currents at +2 V, however, the conductance of this nanopore at −2 V was still the highest in KBr and KI among all salts.

The nanopore shown in Figure 1G,H was 25 nm in diameter; thus as the next step we probed how the opening size influenced the pore's ability to respond to the presence of different ions. Figure 2 summarizes ion current recorded for

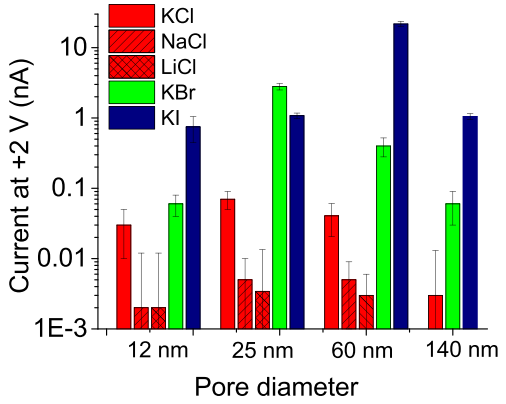

Figure 2. Ionic gating as a function of nanopore diameter. Ionic transport characteristics of nanopores containing a hydrophobic/hydrophilic junction in different 1 M salt solutions. Note that the 140 nm pore was first modified with silanes followed by PAH, thus in reverse order than done for other pores. The error bars are standard deviations found based on ion current signals in time.

four different pores with openings between 12 and 140 nm. At +2 V in KCl, all nanopores were in their low conductance state such that the value of ion current remained below 100 pA independent of the pore opening size. This finding is in agreement with earlier experiments reporting low ion currents through hydrophobic nanopores with an opening of ∼140 nm.[25] All nanopores exhibited significantly higher currents in KBr or KI compared to the recordings in KCl, providing evidence that the large anions facilitated the pores' wetting. We hypothesize that when a pore is wet, a continuous column of electrolyte is created along the pore length, connecting the two reservoirs on both sides of the membrane. It is important to note, however, that the current in KI/KBr shows only a weak dependence on the pore opening diameter, suggesting that the electrolyte does not fill the entire cross-section of the pores. Moreover, the continuous column of electrolyte might not be created along the pore axis, but rather multiple columns of water with possible tortuosity can be present in wider pores.

https://dx.doi.org/10.1021/acsnano.9b09777
ACS Nano 2020, 14, 4306−4315

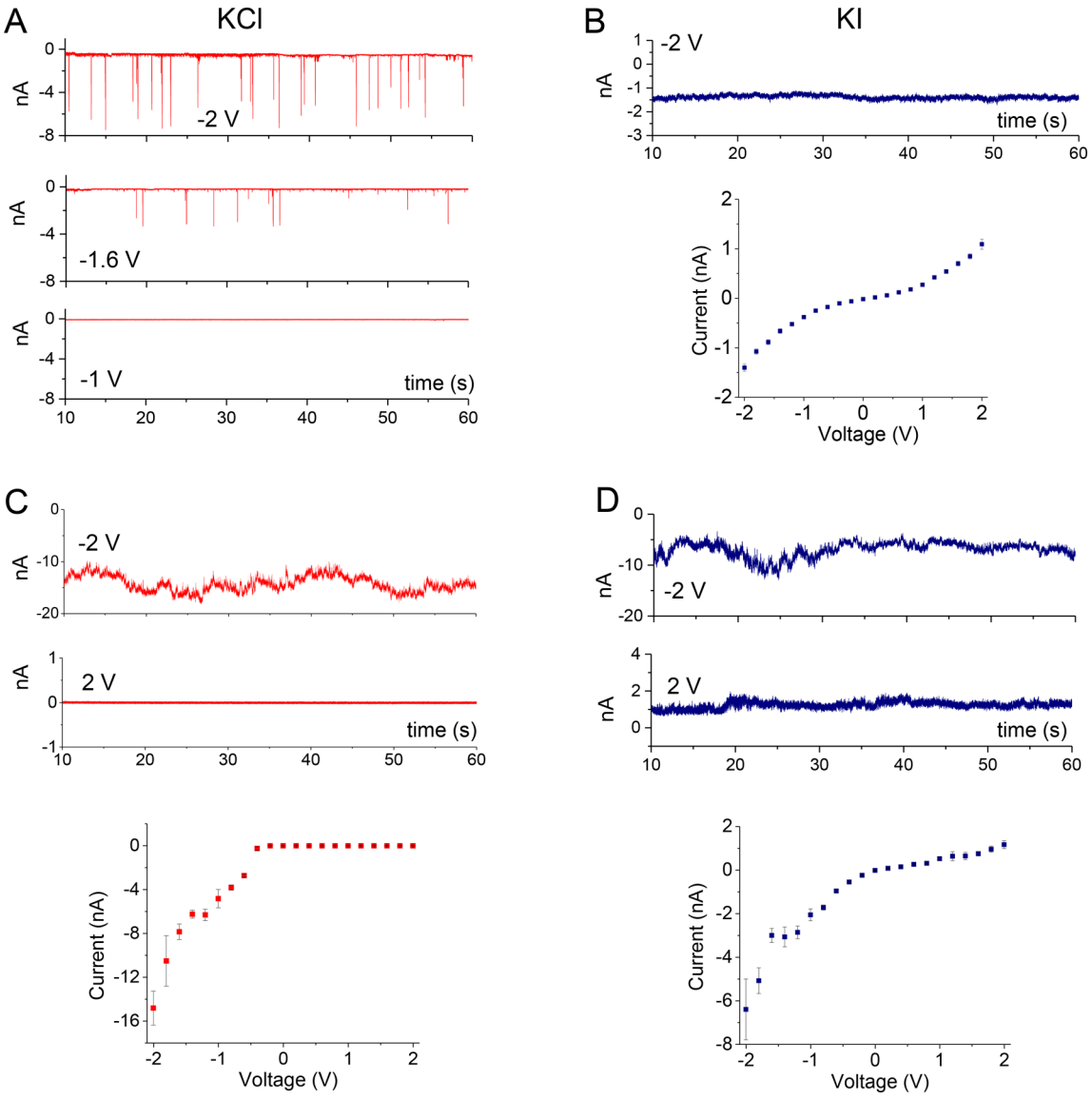

Figure 3. Types of hydrophobic gating. Ion current signals in two nanopores containing a hydrophobic/hydrophilic junction. (A and B) Recordings for a 25 nm diameter pore in 1 M KCl and 1 M KI, respectively. (C and D) Recordings in 1 M KCl and 1 M KI for a 12 nm diameter pore, respectively. Recordings in KCl and KI are presented in red and navy, respectively.

The set of intertwined electrolyte columns would exhibit high ionic resistance and explain the lack of clear dependence of current on the pore diameter, seen in Figure 2.

The change in ion current behavior in KI compared to KCl is even more striking when we compare the characteristics of ion current signals in time. Figure 3 shows ion current recordings in 1 M KCl and 1 M KI for two independently prepared nanopores at different voltages. The pores shown are examples of two types of hydrophobic gating observed in KCl. In the first type of gating, fluctuations of ion current in time were observed for voltages above a certain threshold; the signal would switch between a current value close to 0 nA and a finite current value (Figure 3A); four out of 12 nanopores prepared for this project exhibited this behavior. The number of current instabilities increased with the increase of negative voltage. In the second type of behavior shown (n = 4), ion current also became finite at a threshold negative voltage, but the ion current signals did not exhibit switching behavior (Figure 3C).

Figure 3A shows recordings in KCl for the reverse scan of the 25 nm nanopore shown in Figure 1G that exhibited the first type of gating. When the same pore was exposed to 1 M KI, current fluctuations ceased in the second scan followed by stable current signals for all voltages examined (Figure 3B, Figure S5). The ion current recordings in KI also indicated that the presence of the large anions alone, without external voltage, was not sufficient to induce nanopore wetting; indeed, the contact angle of a hydrophobic surface remained at a constant value of ~105° for all salts (Table S1). The nanopore opens in KI only when an external electric field is applied.

The second type of voltage response in KCl involved a sudden pore opening without significant current fluctuations. Figure 3C provides recordings for a 12 nm diameter pore showing this response. A sudden pore opening in the reverse scan without ion current instabilities was observed at −0.6 V (see current−voltage curve in Figure 3C), and no on−off current switching occurred for higher voltages. When exposed to KI, the nanopore exhibited similar behavior for negative

https://dx.doi.org/10.1021/acsnano.9b09777
ACS Nano 2020, 14, 4306−4315

voltages but opened for transport at positive voltages (Figure 3D).

The ion current recordings in Figure 3 revealed fluctuations whose amplitude significantly exceeds variations in ion current observed with as-prepared nanopores (Figures S1, S3). In order to probe if the current fluctuations were caused by trapped air bubbles, the entire conductivity cell, containing the nanopore and electrolyte solution (1 M KCl), was placed in a vacuum desiccator for 30 min. Figure S6 shows examples of ion current recordings before and after removal of air bubbles. The presence of ion current bursts in both experiments suggests that the ion current instabilities are intrinsic to hydrophobic nanopores.[3,36] We believe the current instabilities arise because the pore is not entirely filled with electrolyte; thus even when the pore is conductive, the continuous electrolyte column (or multiple columns, see above) has a radius that is locally smaller than the geometrical pore opening.[3,36] When voltage is applied, the flow of ions can lead to instabilities in the effective radius of the electrolyte paths, observed as ion current fluctuations.

When analyzing the magnitude of the ion current at negative voltages for both nanopores shown in Figure 3, we realized that at −2 V the pores conduct higher currents in KCl than at KI. In Figure 3A the current bursts at −2 V reach an amplitude of even −7 nA, while in KI the current is only −1.5 nA. The reasoning for this is less clear, but it was observed for multiple devices. Possible explanations stem from the fact that large anions are predicted to adsorb to the silanized pore walls, making the walls effectively negatively charged. This alteration in surface charge distribution could impact measured current.

It should also be noted that three out of 12 pores we prepared did not open for current in KCl for positive or negative voltages; two of the three pores conducted current in KI or/and KBr, which led to finite ion current for both voltage polarities, and one pore was not conductive in any salt. In addition, one nanopore was not successfully modified with hydrophobic silanes, as suggested by the pore's high conductance in KCl for all voltages.

Control experiments were also performed with an unmodified silicon nitride nanopore in KCl, KBr, and KI. These measurements provided evidence that the ion current dependence on voltage and anion type occurred due to the chemical modifications we performed and was not intrinsic to silicon nitride nanopores. Figure S7 shows current−voltage curves for an as-prepared silicon nitride nanopore. As expected, all recordings are linear with similar current magnitudes, in agreement with comparable bulk conductivity of the salts.

The experiments suggested that large polarizable anions enhanced wetting of nanopores containing a junction between a hydrophobic zone and a hydrophilic, positively charged zone. We realized, however, that the anion's effect on ion transport could have two origins: (i) affinity of large anions toward a hydrophobic surface, as mentioned above; or/and (ii) enhanced concentration of anions at the pore entrance containing PAH. The locally enhanced ion concentration could promote wetting, because previous experiments from our group indicated that wetting of hydrophobic nanopores is enhanced in high ionic strength solutions.[23] In order to elucidate which of these phenomena dominates, we prepared a nanopore with one entrance containing a negatively charged polyelectrolyte while the other entrance remained hydrophobic. This system was created by subjecting a nanopore, as schematically shown in Figure 1F, to a solution of polyglutamic acid (PGA). Polyglutamic acid was expected to electrostatically attach to PAH and switch the surface charge from positive to negative. In a control experiment, we confirmed that the attachment of PGA to PAH indeed occurred, as evidenced by a current decrease and inversion of rectification (Figure S8). Figure S9 shows data for a nanopore that was originally 12 nm in diameter and subjected to modification with PAH, silanes, and PGA. This pore exhibited negligible conductance in KCl, NaCl, LiCl, and KBr but opened for ion transport in KI. These experiments provide evidence that the propensity of anions to concentrate at a hydrophobic surface determines the nanopore wetting. It is important to note that the nanopore with PGA was not conductive in KBr, even though hydrophobic nanopores containing positively charged polymer on one side would be open for ionic transport in both KBr and KI. This observation suggested that the effect of preconcentrating anions at the pore entrance might also play a role in the pore wetting.

Our experimental observations on anion-induced wetting of nanopores is consistent with a wide literature on ion-dependent surface tension.[52,53] Surface tension of the water/air interface is known to increase with the addition of inorganic salts such as KCl or KI; however, heavier, more polarizable halides, such as I^-, increase surface tension to a smaller extent than Cl^-. The lower surface tension in I^- salts was explained by accumulation of the anions at the interface. Our hydrophobic nanopores can indeed be wetted in the presence of larger anions and are closed for ionic transport in KCl.

It is also well known that surface tension increases linearly with concentration for a majority of inorganic salts.[54] Consequently, our hydrophobic nanopores are expected to be wetted in less concentrated solutions due to their decreased surface tension. Our earlier results in KCl with hydrophobic nanopores revealed an opposite trend: the nanopores were more prone to become conductive in more concentrated solutions.[23] Preconcentrating of anions by PAH, capable of promoting nanopore wetting, also contradicts the intuition gathered from previous work on surface tension. One nanopore we prepared for this project was probed in 1 M and 100 mM KCl, and a similar trend was observed: the nanopore remained mostly closed in 100 mM KCl (Figure S10). The influence of salt concentration on hydrophobic gating will be probed by us in the future. We believe an explanation of this behavior needs to include the neighboring polar groups as well as application of electric field.

In order to complement and provide insights into our experimental findings, we carried out first-principles molecular dynamics (MD) simulations of chloride, bromide, and iodide ions in bulk water (see Methods section). These simulations provided a detailed understanding on the nature of ion hydration, which can be related to the wetting behavior observed in the experiments. Here, our examination of ion solvation structures was based on the calculated radial distribution functions (RDFs) between the hydrogen atoms in water and the anions, $g_{XH}(r)$, where X = Cl^-, Br^-, or I^-. As shown in Figure 4A, the position of the $g_{XH}(r)$ first maximum, r_X, follows the order $r_{I^-} > r_{Br^-} > r_{Cl^-}$, yielding values of 2.54, 2.35, and 2.17 Å for I^-, Br^-, and Cl^-, respectively. This ordering indicates an increase in the size of the first solvation shell from Cl^- to I^- and reflects the ion radius increase among the three anions. More importantly, the calculated RDFs indicate that Cl^- yields a significantly stronger solvation shell compared to Br^- and I^-, as supported by a shorter average

https://dx.doi.org/10.1021/acsnano.9b09777
ACS Nano 2020, 14, 4306−4315

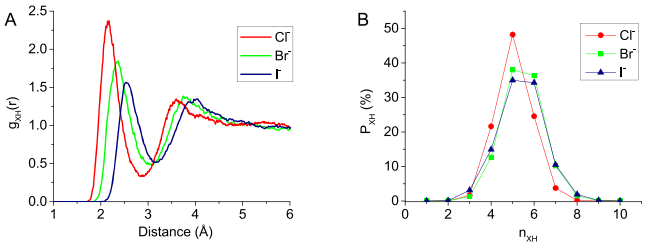

Figure 4. Solvation shell of anions in bulk liquid water. (A) Calculated ion−water hydrogen radial distribution functions for chloride (Cl^-), bromide (Br^-), and iodide (I^-) in bulk water. (B) Histograms of the water hydrogen coordination number in the first shell around the anions. The first minima in the corresponding $g_{XH}(r)$ were used as distance cutoffs for determination of the first solvation shells. The results indicate that large anions yield a weaker and more flexible solvation shell.

ion−hydrogen r_X distance as well as a higher intensity in the $g_{XH}(r)$ first maximum. This analysis also reveals that I^- exhibits the weakest solvation shell among the three anions.

Additional information on the difference in the solvation structures among the ions can be obtained by examining the probability distributions of the ion−hydrogen coordination numbers (n_{XH}). For instance, as shown in Figure 4B, we find that larger ions, such as I^-, exhibit a much broader n_{XH} distribution compared to that of Cl^-. The broad distributions imply that the solvation shells of Br^- and I^- are rather flexible and are characterized by more frequent exchanges of water molecules between the first and second ion solvation shells. Collectively, our simulations support the interpretation of weaker and more flexible solvation shells of Br^- and I^- compared to that of Cl^-, implying that these larger anions are more prone to migrate to hydrophobic surfaces where the water concentration is diminished.

To support this initial assessment, we directly probed adsorption behavior of the anions on a hydrophobic surface. To this end, we carried out MD simulations of KBr, KCl, and KI solutions at the interface with a silicon surface functionalized with flexible silane molecules, where a high surface coverage of 100% was used to represent high hydrophobicity conditions in experiments (Figure 5A,B). In addition, given the complexity of the system, classical simulations were utilized instead of first-principles simulations that require significant computational resource. Here, our simulations were carried out using the TIP3P water model, and OPLS-AA force fields[55] were employed for the description of ions and surface silane molecules (see Methods section). We emphasize that these force fields have been parametrized to recover the experimental hydration energy and solvation structure of the ions in liquid water.[55] In addition, we note that ion surface affinity is largely determined by ion−silane, ion−ion, and ion−water interactions rather than the interactions of ions with the substrate, as aqueous solutions are separated from the silica surface by almost 16 Å (see Figure S11). This distance is larger than the cutoff distance of the OPLS force field employed in our MD simulations; therefore the substrate has only a minor effect on the behavior of ions at the interface.

The calculated density of ions as a function of the distance from the surface is shown in Figure 5C−E. The results indicate that anions with larger ionic radii exhibit stronger adsorption at the interface. In particular, we found that Br^- and I^- are favorably adsorbed at the interface, as indicated by a peak located at a distance of about 6 and 5 Å from the surface,

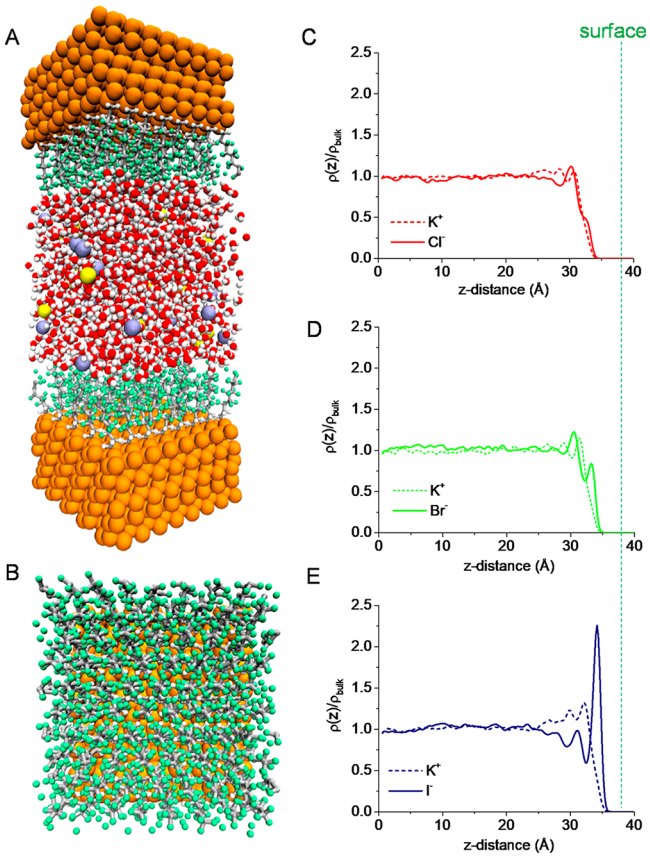

Figure 5. Modeling of ion adsorption at a hydrophobic interface. (A) Side and (B) top view of the atomistic structure of the system composed of silicon surfaces (orange) functionalized with silane molecules (white, silver, and green atoms correspond to hydrogen, carbon, and fluorine, respectively), water (white and red atoms correspond to hydrogen and oxygen, respectively), and ions (yellow cations and blue anions). (C−E) Ion distribution along the direction perpendicular to the surface. The solid and dashed lines show the distributions for the anions and cations for the solutions considered in this work, respectively.

respectively, with the strongest enhancement in interfacial density obtained for I^-. This contrasts with the smaller Cl^- ion, whose distribution reveals depleted density at the interface (Figure 5C). Such an adsorption ordering of the anions can be straightforwardly related to the strength of their solvation assessed in Figure 4. Specifically, larger ions, such as I^-, yield a weak solvation shell, and therefore can be easily desolvated and adsorbed at the hydrophobic interface. In contrast, the smaller ions have a much stronger solvation environment and prefer to remain solvated, preventing them from approaching the interface. The results are in agreement with earlier studies showing that large anions increase surface tension of the water/air interface to a weaker degree compared to smaller anions.[53] Collectively, our simulations indicate that large ions, such as I^-, exhibit a stronger affinity toward hydrophobic surfaces and further support the conclusion that the ions can induce nanopore wetting. We emphasize that our conclusions remain valid for the surface with a lower coverage of silanes (50%), as well as graphene, which can also be considered a model of a hydrophobic system (see Figure S12).[56,57] We also note that the affinity of I^- toward the interface is weaker for the surface with a 50% coverage of silanes due to the decreased hydrophobicity of the surface. As a result, our simulations

https://dx.doi.org/10.1021/acsnano.9b09777
ACS Nano 2020, 14, 4306−4315

suggest that the details of the ion distribution are strongly dependent on the chemical characteristics of the surface.

We also used the electronic continuum correction (ECC) to investigate the effect of polarizability on the behaviors of ions at the interface, where we confirmed that the trend in the surface affinity among the three ions remains the same. Interestingly, we found that the use of the ECC approximation increases surface affinity of all the anions; for instance, the interfacial density of chloride was found to be significantly larger than the bulk density in the ECC simulations (Figure S13). This is likely to be a consequence of the discontinuity in the electronic relative permittivity at the interface between the solutions and silane molecules, which has also been found to be responsible for an overestimation of ionic surface affinity in simulations of the water/vapor interface with the ECC approximation.[58] We note that the ECC approximation is known to be more suitable for systems that are electronically homogeneous, such as the water/oil interface, and is less applicable for those with a discontinuity in the electronic relative permittivity.

The distribution of ions in Figure 5 also shows that an enhanced concentration of I^- at the surface leads to formation of a neighboring region with enhanced concentration of potassium ions, an effect shown before.[28] The two peaks corresponding to anions at the surface and cations resemble properties of an electrical double layer with a distinction that in the case presented here the ionic distributions are governed by hydrophobic properties of the surface and solvation shell of ions in a solution, instead of charges on the surface.[59]

CONCLUSIONS

In this article we examined single nanopores containing a junction between a hydrophobic region and a hydrophilic, highly charged region. The presence of the junction made the system responsive not only to applied voltage but also to the type of ions present in the solution. Our experiments and modeling provided evidence that bromide and iodide ions, due to their weaker solvation shell, had a tendency to accumulate at hydrophobic surfaces and promoted nanopore wetting.

Earlier continuum modeling showed that iodide ions could indeed accumulate at a hydrophobic surface, which was captured by so-called hydrophobic solvation energy related with the ion volume.[28] Our results provide a detailed physical mechanism, which describes effects governing location of ions near a hydrophobic interface. It is the strength of the ion solvation shell that determines whether an ion will have an enhanced or diminished density at a hydrophobic surface. In the confined geometry of a nanopore, which does not *de facto* contain a bulk phase, small ions with strong hydration shells might not even enter the pore. On the other hand, large polarizable ions will accumulate next to hydrophobic walls and induce ionic transport through the nanopore. The importance of ion solvation for ionic distributions near a hydrophobic surface is in strong contrast with a charged surface, where charged chemical groups play a dominant role in modulating local ionic concentrations.[59]

The results presented here will be of great interest in preparing ion-responsive systems based on hydrophobic pores. We also imagine it should be possible to prepare a valve-like membrane, which becomes open for ionic and molecular transport when a threshold voltage or/and gating ion is added. Our future studies will focus on understanding the role of ionic concentration in the hydrophobic gating and introducing electric fields into modeling of hydrophobic interfaces. The experiments and modeling will also be extended to more types of anions and cations. It will be especially important to understand the role of cation and anion affinity to a hydrophobic surface when it is connected to a highly charged zone, as done in the system shown here. It is possible that the adsorption of large ions at a hydrophobic surface is influenced by the presence and polarity of the nearby charges. These experiments will involve probing different salts individually as well as in mixtures.

MATERIALS AND METHODS

The following reagents were purchased from the indicated company and used as received: potassium chloride (KCl, 99.8%, Fisher Scientific), potassium bromide (KBr, infrared grade, Fisher Scientific), potassium iodide (KI, ≥99%, Fisher Scientific), sodium chloride (NaCl, ≥99%, Fisher Scientific), lithium chloride (LiCl, 99%, EMD Chemicals), tris(hydroxymethyl)aminomethane (Tris, 99.9%, Sigma-Aldrich), poly(allylamine hydrochloride) (PAH, MW ≈ 17 500, Sigma-Aldrich), poly-L-glutamic acid sodium salt (PGA, MW ≈ 93 600, Pilot Chemicals), 1*H*,1*H*,2*H*,2*H*-perfluorooctyltrichlorosilane (hydrophobic silane, 97%, Alfa Aesar), hydrogen peroxide (H_2O_2, 30% w/w, Sigma-Aldrich), sulfuric acid (H_2SO_4, 95−98%, VWR). All solutions were made in Milli-Q water (18.2 MΩ). Low-stress silicon nitride membranes (SiN_x, 50 × 50 μm, 30 ± 2 nm thick) were purchased from Norcada and cleaned with piranha solution (3:1, H_2SO_4/H_2O_2) at 100 °C for 30 min prior to pore fabrication.

Pore Fabrication. Silicon nitride films (30 nm thick, 50 × 50 μm^2, Norcada) were subjected to the dielectric breakdown process to fabricate single nanopores.[41] Dielectric breakdown was performed in a homemade polydimethylsiloxane conductivity cell. Larger pores (opening diameter >20 nm) underwent dielectric breakdown with the top half exposed to a strongly basic solution of 1 M KCl (pH 13.1) and the bottom half exposed to a strongly acidic solution of 1 M KCl (pH 1.6). In order to prepare smaller pores (opening diameter <20 nm), both sides were exposed to the pH 1.6 solution. Dielectric breakdown was performed by applying 11.2 V (larger pores) or 12 V (smaller pores) with two Ag/AgCl pellet electrodes. Pore formation was observed as an increase of the current recorded during the dielectric breakdown process by ∼20−1200 nA above the base current. Effective pore diameter was estimated using the pore resistance from an $I-V$ curve in 1 M KCl at pH 8 and assuming a cylindrical geometry of the pore. The total resistance of the pore system is a sum of the access resistance and geometrical pore resistance;[60] thus the opening diameter (D) can be calculated using the following equation:[42]

$$D = \frac{G}{2\sigma}\left[1 + \sqrt{1 + \frac{16\sigma L}{\pi G}}\right]$$

where σ is the solution conductivity, L is pore length (30 nm), and G is the pore conductance determined by the slope of the $I-V$ curve. We consider the calculated value of D as an effective pore diameter.

Pore Modification with PAH and Hydrophobic Silanes. Once fabricated, the pores were first modified with a positive polyelectrolyte (PAH), followed by modification with hydrophobic silanes. In the first step, a nanopore was placed in a conductivity cell; one side of the membrane was exposed to a ∼7 mM solution of PAH in pH 6 water for 30 min; the other side of the conductivity cell contained water. Successful PAH modification was assessed by a decrease of transmembrane current and the presence of ion current rectification. After a thorough drying of the chip, the same pore was subsequently subjected to the modification with 1*H*,1*H*,2*H*,2*H*-perfluoro-octyltrichlorosilane performed from the opposite side of the membrane, previously in contact with water. The modification was performed from a 0.2% silane solution in toluene for 5 min, followed by washing the whole pore in ethanol and heating it at 120 °C for 30 min. Successful silane modification showed a large decrease in the nanopore conductance in KCl. In order to estimate the thickness of

https://dx.doi.org/10.1021/acsnano.9b09777
ACS Nano 2020, 14, 4306−4315

the silane layer, two nanopores were modified with silanes from both sides and submerged in ethanol overnight. They were subsequently characterized in a 1:1 mixture of 1 M KCl and ethanol. In the presence of ethanol, the nanopores were wet and their $I-V$ curves informed on the effective pore size and the silane layer thickness. The calculations were performed assuming a homogeneous thickness of the layer on the pore wall and membrane surface.[61] Once wetted, the nanopores were also characterized in 1 M aqueous KCl, and the thickness was estimated again. Example recordings of current−voltage curves before and after silanization are included in Figure S14. Based on all recordings the silane layer is estimated to be ∼5 nm thick.

Additional Pore Modification with PGA. After PAH and silane modification, a few pores were modified with an additional polyelectrolyte to yield a negatively charged surface at one pore entrance, while the other entrance remained hydrophobic. For these select pores, the bottom of the chip containing PAH was exposed to a ∼0.35 mM solution of PGA in pH 8 water for 30 min while the other side of the membranes was in contact with water.

Electrochemical Measurements. Current−voltage curves were recorded with an Axopatch 200B and Digidata 1322A (Molecular Devices Inc.) from −2 V to +2 V using 200 mV steps and a sampling frequency of 10 kHz. Current at each voltage step was recorded for 100 s, and reported values are averages and standard deviations of the time series excluding the first and last ∼5 s for each voltage. A few measurements of current−voltage curves were performed with a Keithley 6487 picoammeter/voltage source (Keithley Instruments, Cleveland, OH, USA); average and standard deviations were calculated based on three subsequent voltage scans. Pellet Ag/AgCl electrodes were used in all current experiments, with the ground electrode placed at the side of the nanopore modified with silanes. All salt solutions were prepared with 10 mM Tris buffer and adjusted to pH 8.

Contact Angle Measurements. Contact angle measurements were performed using a homemade imaging setup at room temperature. A micropipette tip was filled with 2 μL of solution and dispensed on the SiN_x membrane. Images were captured on a VRI Phantom v7.3 camera outfitted with an Infinity Photo-Optical model K2 DistaMax long-distance microscope. Contact angle values were calculated using the ImageJ contact angle plugin by M. Brugnara.

First-Principles and Classical Simulations. For the simulations of ions in bulk liquid water, all solutions were modeled by periodic cubic cells consisting of 63 water molecules and a single solvated ion, with the excess charge compensated by a uniform background charge. The size of the cells was chosen to yield the experimental density of liquid water under ambient conditions. Our first-principles simulations were carried out using Born−Oppenheimer MD with the Qbox code,[62] with the interatomic force derived from density functional theory (DFT) and the Perdew, Burke, and Ernzerhof (PBE) approximation for the exchange−correlation energy functional.[63] The interaction between valence electrons and ionic cores was represented by norm-conserving pseudopotentials,[64] and the electronic wave functions were expanded in a plane-wave basis set truncated at a cutoff energy of 85 Ry. All hydrogen atoms were replaced with deuterium to maximize the allowable time step, which was chosen to be 10 atomic units. The equilibration runs were carried out at an elevated temperature of T = 400 K in order to recover the experimental water structure and diffusion, while also providing a good description of the ion solvation at room temperature.[40,65−67] For the analysis of structural properties, the statistics were collected over 45 ps microcanonical simulations after an equilibration run of 15 ps.

Classical MD simulations of the hydrophobic interfaces were carried out using the LAMMPS simulation package.[68] The simulation systems consist of an aqueous solution (KBr, KCl, or KI) confined between two parallel Si(111) surfaces that are functionalized with flexible silane molecules. The lateral dimensions of the simulation cell are about 3 nm × 3 nm, and the separation distance between the two surfaces is approximately 7.8 nm from the tips of silane groups after the structures are equilibrated. The confined region was solvated by TIP3P water molecules, and the ions were added to obtain an experimental concentration of 1 M. We employed OPLS-AA force fields for the description of ions and CF_n groups of silane molecules.[55,69] The systems were first energy minimized and then equilibrated for 1 ns under the NPT ensemble by using a Berendsen barostat.[70] The production simulations were run for 30 ns under the NVT ensemble, where a Nosé−Hoover thermostat[71,72] was used to maintain the temperature at 298.15 K. The hydrogen bonds of water molecules were constrained by using the SHAKE algorithm,[73] and the long-range electrostatic interactions were computed using the particle−particle particle−mesh method.[74]

ASSOCIATED CONTENT

Supporting Information

The Supporting Information is available free of charge at https://pubs.acs.org/doi/10.1021/acsnano.9b09777.

Additional experimental recordings of ion transport through hydrophobic nanopores and results of molecular dynamics modeling (PDF)

AUTHOR INFORMATION

Corresponding Authors

Zuzanna S. Siwy − *Department of Chemistry, Department of Physics and Astronomy, and Department of Biomedical Engineering, University of California, Irvine, California 92697, United States;* orcid.org/0000-0003-2626-7873; Phone: 949-824-8290; Email: zsiwy@uci.edu

Tuan Anh Pham − *Quantum Simulations Group and Laboratory for Energy Applications for the Future, Lawrence Livermore National Laboratory, Livermore, California 94551, United States;* orcid.org/0000-0003-0025-7263; Phone: 925-423-6501; Email: pham16@llnl.gov

Authors

Jake W. Polster − *Department of Chemistry, University of California, Irvine, California 92697, United States*

Elif Turker Acar − *Department of Chemistry, University of California, Irvine, California 92697, United States; Department of Chemistry, Faculty of Engineering, Istanbul University - Cerrahpasa, 34320 Istanbul, Turkey*

Fikret Aydin − *Quantum Simulations Group and Laboratory for Energy Applications for the Future, Lawrence Livermore National Laboratory, Livermore, California 94551, United States*

Cheng Zhan − *Quantum Simulations Group and Laboratory for Energy Applications for the Future, Lawrence Livermore National Laboratory, Livermore, California 94551, United States*

Complete contact information is available at: https://pubs.acs.org/10.1021/acsnano.9b09777

Notes

The authors declare no competing financial interest.

ACKNOWLEDGMENTS

This work was supported as part of the Center for Enhanced Nanofluidic Transport, an Energy Frontier Research Center funded by the U.S. Department of Energy, Office of Science, Basic Energy Sciences, under Award No. DE-SC0019112. Work at LLNL was performed under the auspices of the U.S. Department of Energy by Lawrence Livermore National Laboratory under Contract DE-AC52-07NA27344. Computational resources were from the Lawrence Livermore National Laboratory Institutional Computing Grand Challenge Program. E.T.A. acknowledges the Scientific and Technological

Research Council of Turkey (TUBITAK), 2219-International Postdoctoral Research Fellowship Program (App. No. 1059B191600613), and the Istanbul University Cerrahpasa, Engineering Faculty Chemistry Department, for additional financial support. We are grateful to Prof. Peter Taborek and Dr. David Mallin for their help in contact angle measurements. We are grateful to Prof. Mark S. P. Sansom and Prof. Stephen J. Tucker from the University of Oxford for discussions.

REFERENCES

(1) Anishkin, A.; Akitake, B.; Kamaraju, K.; Chiang, C. S.; Sukharev, S. Hydration Properties of Mechanosensitive Channel Pores Define the Energetics of Gating. *J. Phys.: Condens. Matter* **2010**, *22*, 454120.
(2) Anishkin, A.; Sukharev, S. Water Dynamics and Dewetting Transitions in the Small Mechanosensitive Channel Mscs. *Biophys. J.* **2004**, *86*, 2883−2895.
(3) Beckstein, O.; Sansom, M. S. P. Liquid−Vapor Oscillations of Water in Hydrophobic Nanopores. *Proc. Natl. Acad. Sci. U. S. A.* **2003**, *100*, 7063−7068.
(4) Beckstein, O.; Sansom, M. S. P. A Hydrophobic Gate in an Ion Channel: The Closed State of the Nicotinic Acetylcholine Receptor. *Phys. Biol.* **2006**, *3*, 147−159.
(5) Aryal, P.; Sansom, M. S. P.; Tucker, S. J. Hydrophobic Gating in Ion Channels. *J. Mol. Biol.* **2015**, *427*, 121−130.
(6) Yonkunas, M.; Kurnikova, M. The Hydrophobic Effect Contributes to the Closed State of a Simplified Ion Channel through a Conserved Hydrophobic Patch at the Pore-Helix Crossing. *Front. Pharmacol.* **2015**, *6*, 284.
(7) Willard, A. P.; Chandler, D. The Molecular Structure of the Interface between Water and a Hydrophobic Substrate Is Liquid-Vapor Like. *J. Chem. Phys.* **2014**, *141*, 18C519.
(8) Stillinger, F. H. Structure in Aqueous Solutions of Nonpolar Solutes from the Standpoint of Scaled-Particle Theory. *J. Solution Chem.* **1973**, *2*, 141−158.
(9) Chandler, D. Interfaces and the Driving Force of Hydrophobic Assembly. *Nature* **2005**, *437*, 640−647.
(10) Remsing, R. C.; Rodgers, J. M.; Weeks, J. D. Deconstructing Classical Water Models at Interfaces and in Bulk. *J. Stat. Phys.* **2011**, *145*, 313−334.
(11) Patel, A. J.; Varilly, P.; Chandler, D. Fluctuations of Water near Extended Hydrophobic and Hydrophilic Surfaces. *J. Phys. Chem. B* **2010**, *114*, 1632−1637.
(12) Patel, A. J.; Varilly, P.; Jamadagni, S. N.; Hagan, M. F.; Chandler, D.; Garde, S. Sitting at the Edge: How Biomolecules Use Hydrophobicity to Tune Their Interactions and Function. *J. Phys. Chem. B* **2012**, *116*, 2498−2503.
(13) Brown, M. A.; D'Auria, R.; Kuo, I. F. W.; Krisch, M. J.; Starr, D. E.; Bluhm, H.; Tobias, D. J.; Hemminger, J. C. Ion Spatial Distributions at the Liquid−Vapor Interface of Aqueous Potassium Fluoride Solutions. *Phys. Chem. Chem. Phys.* **2008**, *10*, 4778−4784.
(14) Liu, D.; Ma, G.; Levering, L. M.; Allen, H. C. Vibrational Spectroscopy of Aqueous Sodium Halide Solutions and Air−Liquid Interfaces: Observation of Increased Interfacial Depth. *J. Phys. Chem. B* **2004**, *108*, 2252−2260.
(15) Petersen, P. B.; Saykally, R. J. Probing the Interfacial Structure of Aqueous Electrolytes with Femtosecond Second Harmonic Generation Spectroscopy. *J. Phys. Chem. B* **2006**, *110*, 14060−14073.
(16) Jungwirth, P.; Tobias, D. J. Molecular Structure of Salt Solutions: A New View of the Interface with Implications for Heterogeneous Atmospheric Chemistry. *J. Phys. Chem. B* **2001**, *105*, 10468−10472.
(17) Dang, L. X.; Chang, T.-M. Molecular Mechanism of Ion Binding to the Liquid/Vapor Interface of Water. *J. Phys. Chem. B* **2002**, *106*, 235−238.
(18) Dang, L. X. Computational Study of Ion Binding to the Liquid Interface of Water. *J. Phys. Chem. B* **2002**, *106*, 10388−10394.
(19) Tian, C.; Byrnes, S. J.; Han, H.-L.; Shen, Y. R. Surface Propensities of Atmospherically Relevant Ions in Salt Solutions Revealed by Phase-Sensitive Sum Frequency Vibrational Spectroscopy. *J. Phys. Chem. Lett.* **2011**, *2*, 1946−1949.
(20) Petersen, P. B.; Saykally, R. J. On the Nature of Ions at the Liquid Water Surface. *Annu. Rev. Phys. Chem.* **2006**, *57*, 333−364.
(21) Ghosal, S.; Hemminger, J. C.; Bluhm, H.; Mun, B. S.; Hebenstreit, E. L. D.; Ketteler, G.; Ogletree, D. F.; Requejo, F. G.; Salmeron, M. Electron Spectroscopy of Aqueous Solution Interfaces Reveals Surface Enhancement of Halides. *Science* **2005**, *307*, 563−566.
(22) Vrbka, L.; Mucha, M.; Minofar, B.; Jungwirth, P.; Brown, E. C.; Tobias, D. J. Propensity of Soft Ions for the Air/Water Interface. *Curr. Opin. Colloid Interface Sci.* **2004**, *9*, 67−73.
(23) Innes, L.; Gutierrez, D.; Mann, W.; Buchsbaum, S. F.; Siwy, Z. S. Presence of Electrolyte Promotes Wetting and Hydrophobic Gating in Nanopores with Residual Surface Charges. *Analyst* **2015**, *140*, 4804−4812.
(24) Powell, M. R.; Cleary, L.; Davenport, M.; Shea, K. J.; Siwy, Z. S. Electric-Field-Induced Wetting and Dewetting in Single Hydrophobic Nanopores. *Nat. Nanotechnol.* **2011**, *6*, 798−802.
(25) Smirnov, S. N.; Vlassiouk, I. V.; Lavrik, N. V. Voltage-Gated Hydrophobic Nanopores. *ACS Nano* **2011**, *5*, 7453−7461.
(26) Setny, P.; Baron, R.; Michael Kekenes-Huskey, P.; McCammon, J. A.; Dzubiella, J. Solvent Fluctuations in Hydrophobic Cavity−Ligand Binding Kinetics. *Proc. Natl. Acad. Sci. U. S. A.* **2013**, *110*, 1197−1202.
(27) Hulteen, J. C.; Jirage, K. B.; Martin, C. R. Introducing Chemical Transport Selectivity into Gold Nanotubule Membranes. *J. Am. Chem. Soc.* **1998**, *120*, 6603−6604.
(28) Huang, D. M.; Cottin-Bizonne, C.; Ybert, C.; Bocquet, L. Ion-Specific Anomalous Electrokinetic Effects in Hydrophobic Nanochannels. *Phys. Rev. Lett.* **2007**, *98*, 177801.
(29) Bratko, D.; Daub, C. D.; Leung, K.; Luzar, A. Effect of Field Direction on Electrowetting in a Nanopore. *J. Am. Chem. Soc.* **2007**, *129*, 2504−2510.
(30) Michelin-Jamois, M.; Picard, C.; Vigier, G.; Charlaix, E. Giant Osmotic Pressure in the Forced Wetting of Hydrophobic Nanopores. *Phys. Rev. Lett.* **2015**, *115*, 036101.
(31) Fadeev, A. Y.; Eroshenko, V. A. Study of Penetration of Water into Hydrophobized Porous Silicas. *J. Colloid Interface Sci.* **1997**, *187*, 275−282.
(32) Lefevre, B.; Saugey, A.; Barrat, J. L.; Bocquet, L.; Charlaix, E.; Gobin, P. F.; Vigier, G. Intrusion and Extrusion of Water in Hydrophobic Mesopores. *J. Chem. Phys.* **2004**, *120*, 4927−4938.
(33) Dzubiella, J.; Hansen, J.-P. Electric-Field-Controlled Water and Ion Permeation of a Hydrophobic Nanopore. *J. Chem. Phys.* **2005**, *122*, 234706.
(34) Toney, M. F.; Howard, J. N.; Richer, J.; Borges, G. L.; Gordon, J. G.; Melroy, O. R.; Wiesler, D. G.; Yee, D.; Sorensen, L. B. Voltage-Dependent Ordering of Water Molecules at an Electrode−Electrolyte Interface. *Nature* **1994**, *368*, 444−446.
(35) Shafiei, M.; Domaros, M. v.; Bratko, D.; Luzar, A. Anisotropic Structure and Dynamics of Water Under Static Electric Fields. *J. Chem. Phys.* **2019**, *150*, 074505.
(36) Trick, J. L.; Song, C.; Wallace, E. J.; Sansom, M. S. P. Voltage Gating of a Biomimetic Nanopore: Electrowetting of a Hydrophobic Barrier. *ACS Nano* **2017**, *11*, 1840−1847.
(37) Giovambattista, N.; Debenedetti, P. G.; Rossky, P. J. Hydration Behavior under Confinement by Nanoscale Surfaces with Patterned Hydrophobicity and Hydrophilicity. *J. Phys. Chem. C* **2007**, *111*, 1323−1332.
(38) Ma, C. D.; Wang, C.; Acevedo-Vélez, C.; Gellman, S. H.; Abbott, N. L. Modulation of Hydrophobic Interactions by Proximally Immobilized Ions. *Nature* **2015**, *517*, 347−350.
(39) Cheng, Y.-K.; Rossky, P. J. Surface Topography Dependence of Biomolecular Hydrophobic Hydration. *Nature* **1998**, *392*, 696−699.
(40) Pham, T. A.; Mortuza, S. M. G.; Wood, B. C.; Lau, E. Y.; Ogitsu, T.; Buchsbaum, S. F.; Siwy, Z. S.; Fornasiero, F.; Schwegler, E. Salt Solutions in Carbon Nanotubes: The Role of Cation-π Interactions. *J. Phys. Chem. C* **2016**, *120*, 7332−7338.

https://dx.doi.org/10.1021/acsnano.9b09777
ACS Nano 2020, 14, 4306−4315

(41) Kwok, H.; Briggs, K.; Tabard-Cossa, V. Nanopore Fabrication by Controlled Dielectric Breakdown. *PLoS One* **2014**, *9*, e92880.
(42) Acar, E. T.; Hinkle, P.; Siwy, Z. S. Concentration-Polarization-Induced Precipitation and Ionic Current Oscillations with Tunable Frequency. *J. Phys. Chem. C* **2018**, *122*, 3648−3654.
(43) Arcadia, C. E.; Reyes, C. C.; Rosenstein, J. K. *In Situ* Nanopore Fabrication and Single-Molecule Sensing with Microscale Liquid Contacts. *ACS Nano* **2017**, *11*, 4907−4915.
(44) Smirnov, S.; Vlassiouk, I.; Takmakov, P.; Rios, F. Water Confinement in Hydrophobic Nanopores. Pressure-Induced Wetting and Drying. *ACS Nano* **2010**, *4*, 5069−5075.
(45) Agazzi, M. L.; Herrera, S. E.; Cortez, M. L.; Marmisollé, W. A.; von Bilderling, C.; Pietrasanta, L. I.; Azzaroni, O. Continuous Assembly of Supramolecular Polyamine−Phosphate Networks on Surfaces: Preparation and Permeability Properties of Nanofilms. *Soft Matter* **2019**, *15*, 1640−1650.
(46) Vlassiouk, I.; Kozel, T. R.; Siwy, Z. S. Biosensing with Nanofluidic Diodes. *J. Am. Chem. Soc.* **2009**, *131*, 8211−8220.
(47) Vlassiouk, I.; Smirnov, S.; Siwy, Z. Nanofluidic Ionic Diodes. Comparison of Analytical and Numerical Solutions. *ACS Nano* **2008**, *2*, 1589−1602.
(48) Nguyen, G.; Vlassiouk, I.; Siwy, Z. S. Comparison of Bipolar and Unipolar Ionic Diodes. *Nanotechnology* **2010**, *21*, 265301.
(49) Karnik, R.; Duan, C.; Castelino, K.; Daiguji, H.; Majumdar, A. Rectification of Ionic Current in a Nanofluidic Diode. *Nano Lett.* **2007**, *7*, 547−551.
(50) Siwy, Z. S.; Howorka, S. Engineered Voltage-Responsive Nanopores. *Chem. Soc. Rev.* **2010**, *39*, 1115−1132.
(51) Tinti, A.; Giacomello, A.; Grosu, Y.; Casciola, C. M. Intrusion and Extrusion of Water in Hydrophobic Nanopores. *Proc. Natl. Acad. Sci. U. S. A.* **2017**, *114*, E10266−E10273.
(52) Petersen, P. B.; Saykally, R. J. On the Nature of Ions at the Liquid Water Surface. *Annu. Rev. Phys. Chem.* **2006**, *57*, 333−364.
(53) Jungwirth, P.; Tobias, D. J. Ions at the Air/Water Interface. *J. Phys. Chem. B* **2002**, *106*, 6361−6373.
(54) Chattoraj, D. K.; Birdi, K. S. Adsorption at Liquid Interfaces and the Gibbs Equation. In *Adsorption and the Gibbs Surface Excess*; Plenum Press: New York, 1984; pp 39−81.
(55) Jorgensen, W. L.; Maxwell, D. S.; Tirado-Rives, J. Development and Testing of the Opls All-Atom Force Field on Conformational Energetics and Properties of Organic Liquids. *J. Am. Chem. Soc.* **1996**, *118*, 11225−11236.
(56) McCaffrey, D. L.; Nguyen, S. C.; Cox, S. J.; Weller, H.; Alivisatos, A. P.; Geissler, P. L.; Saykally, R. J. Mechanism of Ion Adsorption to Aqueous Interfaces: Graphene/Water *vs.* Air/Water. *Proc. Natl. Acad. Sci. U. S. A.* **2017**, *114*, 13369−13373.
(57) Sala, J.; Guardia, E.; Marti, J. Specific Ion Effects in Aqueous Eletrolyte Solutions Confined within Graphene Sheets at the Nanometric Scale. *Phys. Chem. Chem. Phys.* **2012**, *14*, 10799−10808.
(58) Vazdar, M.; Pluhařová, E.; Mason, P. E.; Vácha, R.; Jungwirth, P. Ions at Hydrophobic Aqueous Interfaces: Molecular Dynamics with Effective Polarization. *J. Phys. Chem. Lett.* **2012**, *3*, 2087−2091.
(59) Schoch, R. B.; Han, J. Y.; Renaud, P. Transport Phenomena in Nanofluidics. *Rev. Mod. Phys.* **2008**, *80*, 839−883.
(60) Hall, J. E. Access Resistance of a Small Circular Pore. *J. Gen. Physiol.* **1975**, *66*, 531.
(61) Lin, K.; Lin, C.-Y.; Polster, J. W.; Chen, Y.; Siwy, Z. S. Charge Inversion and Calcium Gating in Mixtures of Ions in Nanopores. *J. Am. Chem. Soc.* **2020**, *142*, 2925−2934.
(62) Gygi, F. Architecture of Qbox: A Scalable First-Principles Molecular Dynamics Code. *IBM J. Res. Dev.* **2008**, *52*, 137−144.
(63) Perdew, J. P.; Burke, K.; Ernzerhof, M. Generalized Gradient Approximation Made Simple. *Phys. Rev. Lett.* **1996**, *77*, 3865−3868.
(64) Schlipf, M.; Gygi, F. Optimization Algorithm for the Generation of ONCV Pseudopotentials. *Comput. Phys. Commun.* **2015**, *196*, 36−44.
(65) Pham, T. A.; Ogitsu, T.; Lau, E. Y.; Schwegler, E. Structure and Dynamics of Aqueous Solutions from PBE-Based First-Principles Molecular Dynamics Simulations. *J. Chem. Phys.* **2016**, *145*, 154501.
(66) Grossman, J. C.; Schwegler, E.; Draeger, E. W.; Gygi, F.; Galli, G. Towards an Assessment of the Accuracy of Density Functional Theory for First Principles Simulations of Water. *J. Chem. Phys.* **2004**, *120*, 300−311.
(67) Schwegler, E.; Grossman, J. C.; Gygi, F.; Galli, G. Towards an Assessment of the Accuracy of Density Functional Theory for First Principles Simulations of Water. II. *J. Chem. Phys.* **2004**, *121*, 5400−5409.
(68) Plimpton, S. Fast Parallel Algorithms for Short-Range Molecular Dynamics. *J. Comput. Phys.* **1995**, *117*, 1−19.
(69) Watkins, E. K.; Jorgensen, W. L. Perfluoroalkanes: Conformational Analysis and Liquid-State Properties from *Ab Initio* and Monte Carlo Calculations. *J. Phys. Chem. A* **2001**, *105*, 4118−4125.
(70) Berendsen, H. J. C.; Postma, J. P. M.; Vangunsteren, W. F.; Dinola, A.; Haak, J. R. Molecular-Dynamics with Coupling to an External Bath. *J. Chem. Phys.* **1984**, *81*, 3684−3690.
(71) Nosé, S. A Unified Formulation of the Constant Temperature Molecular Dynamics Methods. *J. Chem. Phys.* **1984**, *81*, 511−519.
(72) Hoover, W. G. Canonical Dynamics - Equilibrium Phase-Space Distributions. *Phys. Rev. A: At., Mol., Opt. Phys.* **1985**, *31*, 1695−1697.
(73) Ryckaert, J.-P.; Ciccotti, G.; Berendsen, H. J. C. Numerical Integration of the Cartesian Equations of Motion of a System with Constraints: Molecular Dynamics of N-Alkanes. *J. Comput. Phys.* **1977**, *23*, 327−341.
(74) Hockney, R. W.; Eastwood, J. W. *Computer Simulation Using Particles*; CRC Press: Boca Raton, 1988.

https://dx.doi.org/10.1021/acsnano.9b09777
ACS Nano 2020, 14, 4306−4315